



Published in final edited form as:

Neuroimage. 2009 October 1; 47(4): . doi:10.1016/j.neuroimage.2009.06.017.

Physiologically Evoked Neuronal Current MRI in a Bloodless Turtle Brain

Qingfei Luo^{*}, Huo Lu[†], Hanbing Lu[‡], David Senseman[§], Keith Worsley[¶], Yihong Yang[‡], and Jia-Hong Gao^{*}

^{*}Brain Research Imaging Center, The University of Chicago, Chicago, IL 60637

[†]Research Imaging Center, The University of Texas Health Science Center, San Antonio, TX 78229

[‡]National Institute on Drug Abuse, National Institutes of Health, Baltimore, MD 21224

[§]Department of Biology, The University of Texas, San Antonio, TX 78249

[¶]Department of Statistics, The University of Chicago, Chicago, IL 60637

Abstract

Contradictory results from the efforts for detecting evoked neuronal currents have left the feasibility of neuronal current MRI (ncMRI) an open question. Most of the previous ncMRI studies in human subjects are suspect due to their inability to separate or eliminate the hemodynamic effects. In this study, we used a bloodless turtle brain that eliminates hemodynamic effects, to explore the feasibility of detecting visual-evoked ncMRI signals at 9.4T. The turtle brain, with its eyes attached, was dissected from the cranium and placed in artificial cerebral spinal fluid. Light flashes were delivered to the eyes, which produced visual-evoked neuronal activity in the brain. Local field potential (LFP) and MRI signals in the turtle brain were measured in an interleaved fashion. Although robust neuronal responses to the visual stimulation were observed in the LFP signals, no significant signal changes synchronized with neuronal currents were found in the MRI images. Analysis of the temporal stability of the MRI time courses indicated that the detectable effect sizes are 0.11% and 0.09° for the magnitude and phase, respectively, and the visual-evoked ncMRI signals in the turtle brain are below these levels.

Advances in non-invasive neuroimaging have greatly enhanced our understanding of the functional organization of the human brain. However, limitations remain in current leading neuroimaging methods. EEG and MEG directly measure neuronal electric activity with high temporal resolution, but afford limited spatial resolution and uncertainty of activation location due to the inverse source problem. Functional MRI (fMRI) and PET techniques detect changes in regional hemodynamic and metabolism (blood flow/volume/oxygenation and glucose metabolism) that accompany changes in neuronal activity. However, due to the variation of vasculature and the complex nature of neuronal-hemodynamic coupling, both fMRI and PET techniques are unable to achieve high spatial and temporal accuracy for mapping neuronal activity.

To overcome the limitations of present neuroimaging methods, researchers have made efforts to use MRI to measure directly the magnetic fields generated by the neuronal electrical activity, termed neuronal current MRI (ncMRI). Neuronal activity generates changes in ionic currents along neuronal axons and dendrites. The ionic currents produce

weak, transient magnetic fields around the neurons. The component of neuronal magnetic fields parallel to the B_0 field of a MRI scanner will change the precession rate of nuclear spins and may induce both coherence phase shift and phase dispersion, which can be measured by the phase and magnitude of MRI signal, respectively. Since ncMRI signal is based on ionic flows that are directly associated with synaptic events and regenerative spikes, it would offer substantial improvement in both spatial and temporal resolutions and therefore provide a more reliable measurement relevant to the fundamental electrophysiological events underlying cognitive processing.

The fundamental question needs to be addressed is not whether ncMRI signals exist, but rather, are they large enough and sufficient coherent to be detectable with current technology. To date, the answer to this question has been equivocal. Successful detection of ncMRI signal on human brain has been reported by several groups (1–9), while others (10–14) have failed to capture the neuronal electric activity using MRI. The discrepancies between these studies could be caused by contamination from hemodynamic effects, which have not been clearly separated from the direct neuronal electric signals in previous human ncMRI studies (15) except in Chu's study (11). In addition, the physiological noise such as cardiac pulsation and respiration in the human subjects may also contribute to the contradictory findings in previous human ncMRI studies.

One obvious way to eliminate the possibility of hemodynamic contamination of the ncMRI signal and physiological noise is to record from neural tissue using an *in vitro* experimental system. This approach has been used recently by two groups to study ncMRI signals, i.e., Park et al. (16, 17) using isolated snail ganglia and Petridou et al. (18) using rat organotypic brain cultures. Both groups reported successfully detecting ncMRI signals in response to either electrical stimulation or pharmacological intervention. While encouraging, these studies leave open the question whether ncMRI signals can be recorded from an intact vertebrate central nervous system in response to normal sensory stimulation?

In this study, we used a bloodless and intact turtle brain to explore the feasibility for detecting the visual-evoked ncMRI signal. After being surgically removed from the cranium and placed in artificial cerebral spinal fluid (aCSF), the turtle brain with the eyes attached is able to display essentially normal electrophysiological activity in response to visual stimulation for 72 hours or more (19, 20). This isolated turtle eye-brain preparation provides a useful animal model for exploring the feasibility of ncMRI techniques. Because of the turtle's resistance to anoxia, it is not only possible to record apparently normal brain electrical activity *in vitro*, but to record this activity from an intact brain in which most, if not all, of the blood has been removed previously by cardiac perfusion with aCSF. Moreover, since the eyes can be left attached to this "bloodless" brain *in vitro*, it becomes possible to study ncMRI signals evoked by natural sensory stimulation.

In the study reported below, we used brief white light flashes to stimulate the turtle eye-brain preparation *in vitro*. Since visual stimulation evokes neuronal activity not only in the dorsal area of the turtle's cerebral cortex, but also the optic tectum (the reptilian homolog of the superior colliculus), we acquired MRI images in both brain areas at a 9.4T MRI scanner. The local field potential (LFP) was recorded using the identical visual stimulation paradigm as used in the ncMRI experiment. The LFP signals provided the temporal information (i.e. peak latency and response duration) for the optimization of the MRI acquisition. To detect the ncMRI signal changes, we compared the MRI images acquired during the time window of the visual-evoked activation (monitored and determined by the LFP signals) with the MRI images collected during baseline.

Results

To produce evoked neuronal activity in the turtle brain, a visual stimulus with duration 50ms was delivered to the eyes every 16s. A total of eight turtles were used to detect the LFP and ncMRI signals generated by the visual evoked neuronal activity.

Visual-evoked LFP signal

LFP signals for the visual-evoked activity were recorded in the visual cortex and optic tectum immediately before and after the MRI session (Figure 1A). During the MRI session, an interleaved LFP/MRI acquisition strategy was used. A single channel LFP signal in the tectum was collected between any two adjacent MRI scans. The LFP signal was measured only at one point in the tectum during the MRI session. This ensured that the susceptibility effects of the silver electrodes would not affect the MRI signals in the visual cortex and most areas of tectum. The purpose of LFP recording was twofold. First, the LFP signals were used to monitor whether the turtle brain responded to the visual stimulation during the MRI scans. Second, the temporal information provided by the time course of visual evoked LFP signal was utilized to optimize the time windows of MRI acquisition.

In all the eight turtle brains, a robust, strong and transient response to the visual stimulation was observed in the LFP traces measured immediately before and after the MRI session, and in the LFP signals that were recorded interleaved with the MRI scans. A typical example of the LFP signals in a turtle is given in Fig. 1B–E. The LFP signals shown in the figure were obtained by averaging the signals of 20 trials. Each trial lasted 16s, which included a stimulus of 50ms followed by a rest period (stimulus off) of 15.95s. The visual-evoked LFP signals were composed of a strong positive peak followed by a weaker negative component. Averaged over the eight turtles, the peak latency (time reach to the peak from the stimulus onset) and the response duration (full width at half maximum of the peak) in the visual cortex (tectum) were $221\pm 36\text{ms}$ ($119\pm 23\text{ms}$) and $205\pm 31\text{ms}$ ($87\pm 15\text{ms}$), respectively. The visual-evoked LFP signals in all the eight turtles completely returned to the baseline within 1.6s after the stimulus onset.

Visual-evoked ncMRI signal

Five slices were selected to cover the whole visual cortex and optic tectum of the turtle brain (Fig. 2A). Based on the LFP time courses obtained prior to the MRI session, a time delay (τ in the range of 25–50ms for eight turtles, and the value of τ was determined for each individual turtle) was set between the start of visual stimulation and MRI acquisition to ensure that the imaging slices at the central cortex (slice 4) and tectum (slice 2) were acquired during their respective positive peaks of neuronal electrical activity (Fig. 2B). The MRI images for six different echo times ($\text{TEs}=15\text{--}40\text{ms}$ with 5ms interval) were acquired in six separate MRI scans, respectively (see Fig. 1A). For an individual TE, 8 images were acquired for each slice with a repetition time (TR) of 2s in each trial, and a total of 140 trials were collected. For each slice, the first image in each trial was acquired during the visual-evoked neuronal activity (active state) and the subsequent seven images in each trial were acquired when the neuronal activity completely returned to the baseline (resting state).

The voxel-wise analysis with multiple comparison correction (see Methods) was used for detecting the ncMRI signal. For each slice and each individual TE, one t-map was obtained by statistically comparing the images at active state and that at resting state. Totally 240 t-maps ($8\text{ turtles} \times 6\text{ TEs} \times 5\text{ slices}$) were produced from the magnitude/phase images. In the 240 t-maps (for both negative and positive signal changes), there were only 11/9 (magnitude/phase) voxels in total above the significance level ($p<0.05$ corrected for multiple comparisons). No more than two voxels exceeded the statistical threshold in any single t-

map. In addition, these 11/9 (magnitude/phase) voxels were randomly distributed in the non-visual brain regions. All these facts implied that the 11/9 voxels resulted from an effect by chance. In other word, the multiple comparison analysis showed that no significant ncMRI signal was detected.

An alternative and less conservative data analysis method was also performed to avoid the possible missing in detection of the weak ncMRI signal. The method used a low statistical threshold ($p < 0.05$ uncorrected) and was termed as fast effect (FE) vs. control (see Methods). For each slice, the FE and control t-maps were obtained by statistically comparing the first and second images to subsequent six images in each trial, respectively. In each trial, only the first image was acquired during the visual-evoked neuronal response, and the second and the subsequent six images were all acquired during the baseline. Thus, it was expected that the ncMRI activation, if measurable, would be present in the FE t-map but not in the control t-map. Fig. 2C shows the typical FE and control t-maps ($p < 0.05$ uncorrected) for negative signal changes overlaid on the T_2 -weighted high-resolution anatomical image. The t-maps were obtained from the magnitude images of $TE = 20$ ms. It can be seen that there are a few voxels above the significance level in the turtle brain, and they are scattered throughout the brain with few clusters in both FE and control t-maps (Fig. 2C). It is found that the spatial distribution and the total number of “activated” voxels (meaning the voxels at $p < 0.05$) in the FE t-maps are comparable to that in the control t-maps. No statistically significant difference was found in terms of the number of “activated” voxels, and percent MRI signal change averaged over the “activated” voxels in the five imaging slices ($n = 8$, see Fig. 2D). Similarly, in the FE and control t-maps for positive signal changes, only a few voxels surpass the p -threshold ($= 0.05$) and are scattered throughout the brain. There are 16 ± 3 and 17 ± 3 “activated” voxels in the FE and control t-maps of the eight turtles, respectively. The average percent MRI signal changes of the “activated” voxels are $0.16 \pm 0.04\%$ and $0.15 \pm 0.03\%$, respectively. Thus, there is no statistically significant difference in the number of “activated” voxels ($p = 0.7$, $n = 8$) and averaged signal change ($p = 0.8$, $n = 8$) for the FE and control t-maps of positive signal changes. The data analysis of magnitude images for other TEs ($TE = 15$ to 40 ms with interval of 5 ms) also reached the same conclusion: the number of “activated voxels” and average signal change did not vary significantly between the FE and control t-maps.

In the phase images, again, there are a few scattered “activated” voxels in both FE and control t-maps for both negative and positive changes. In the FE t-maps of $TE = 20$ ms for negative/positive signal changes, the number of “activated” voxels are $8 \pm 3 / 10 \pm 2$ and the MRI phase signal changes averaged over the “activated” voxels are $-0.12 \pm 0.02^\circ / 0.14 \pm 0.03^\circ$ ($n = 8$). In the corresponding control t-maps, there are $10 \pm 3 / 11 \pm 4$ “activated” voxels and the average phase negative/positive signal changes are $-0.10 \pm 0.03^\circ / 0.13 \pm 0.02^\circ$. The FE t-maps do not significantly differ from the control t-maps in terms of the number of “activated” voxels ($p = 0.5 / 0.7$, $n = 8$) and average MRI phase changes ($p = 0.4 / 0.7$, $n = 8$). The same conclusion was also drawn from the phase images for other TEs.

The results from the voxel-wise data analysis demonstrated that there were no significant differences in “activated” voxels and MRI signal changes between the FE and control t-maps. This suggests that the “activated” voxels shown in the FE t-maps are likely generated by random noise, just as the control t-map does. In the present study, the measured temporal stability ($1 / (\text{temporal signal-to-noise ratio})$) of magnitude/phase MRI image time series was $0.57\% / 0.52^\circ$. Totally 980 time points (140 trials and seven images for each slice in each trial) were used to calculate the FE and control t-maps, and the ratio of the time points at active state to the total number of time points was $1/7$. For this experimental condition, the power analysis (21) estimated that the lowest signal change (effect size) can be detected for

$p < 0.05$ uncorrected would be $0.11\%/0.09^\circ$. The absence of ncMRI activation in the FE t-maps implies that the visual-evoked ncMRI signal should be below $0.11\%/0.09^\circ$.

MRI data was also analyzed in a region-of-interest (ROI) fashion (see Methods). In the ROI analysis for cortex, four ROIs (medial cortex, dorsomedial cortex, medial visual cortex, and lateral visual cortex) were selected to cover the four major cortical areas (schematic drawing of cortex in Fig. 2C), respectively. Each ROI included two sub-regions which correspond to the two parts of a cortical area in left and right brain hemispheres, respectively. The ROI-averaged signals of each cortical area, visual cortex, and whole cortex were obtained by averaging the MRI signals inside each ROI, the ROIs of medial and lateral visual cortex, and all four ROIs. An ROI-averaged signal was composed of 140 trials and 8 data points per trial. In the ROI analysis for tectum, one ROI was selected to cover the tectal tissue (color region in the schematic drawing of tectum in Fig. 2C), and the corresponding ROI-averaged signal was obtained. It is found that in all the ROI-averaged magnitude/phase signals in cortex and tectum of the eight turtles for $TE=20\text{ms}$, the noise levels (standard error of mean) are in the range of $0.02\%–0.04\%/0.01^\circ–0.03^\circ$, while the signal changes at active state (including the first data point in each trial) relative to resting state (including data points 2–8 in each trial) are all lower than $0.01\%/0.01^\circ$. Therefore, the signal changes are below the noise level, and there is no statistically significant difference between the signals at active state and those at resting state. Fig. 2F and 2E show an example of ROI-averaged signals averaged over the 140 trials in the visual cortex and tectum of one turtle ($TE=20\text{ms}$). It is shown that the signal changes in magnitude/phase at the first data point (active state) relative to the data points 2–8 (resting state) are below the noise level. However, the corresponding LFP traces (averaged over 20 trials) of the visual cortex and tectum (Fig. 2H and 2G) demonstrate that there are strong visual-evoked neuronal activity during the time windows of the first data points in the MRI time courses (Fig. 2F and 2E). This suggests that the visual-evoked neuronal electrical activity was produced in the turtle's cortex and tectum, but the ncMRI signals associated with the neuronal activity were too small to be detected. The ROI analysis on the images for other TEs also reached the same conclusion.

Discussion

Using the turtle eye-brain preparation, we investigated the feasibility of detecting ncMRI signals in the absence of hemodynamic effects and physiological noise such as cardiac pulsation and respiration. We found that the visual-evoked neuronal currents did not result in measurable and significant MRI signal (magnitude and phase) changes. This suggests that the ncMRI signal induced by normal sensory stimulation could be too small to be measured with current detection methods. In the present study, we acquired the MRI images at high magnetic field (9.4T) with localized surface receiving coil, and used 980 time points for calculating the t-maps. This allowed us to detect an ncMRI magnitude/phase signal change as low as $0.11\%/0.09^\circ$ ($p < 0.05$). The absence of ncMRI signal measured in this study suggests that the visual-evoked ncMRI signals are lower than $0.11\%/0.09^\circ$.

A difference of 10,000–100,000 times exists in the order of ncMRI signal changes predicted by different theoretical models and phantoms studies (22–28). Optimistic models (25, 27) predict that the ncMRI signal changes in magnitude (phase) can reach up to the order of 1% (1 degree), while conservative models (26, 28) estimate that the ncMRI signal changes in magnitude (phase) are on the order of 10^{-7} (10^{-4} degree). If the conservative models are valid, the present MRI technology is not able to measure a signal change of 10^{-7} (10^{-4} degree) in a practical way. If the optimistic model (27) was used to estimate the visual-evoked ncMRI signal changes in our experimental condition ($TE=20\text{ms}$), it would be approximately 0.32% in magnitude and 0.21 degree in phase. Our experimental strategy allowed the detection of ncMRI signal changes in magnitude (phase) above 0.11% (0.09

degree). The absence of the measurable ncMRI signal in our study implied that the optimistic models have overestimated the ncMRI signal changes.

The unique feature of the turtle eye-brain experiments presented in this study is the ability to preserve the entire visual system and brain neural network, allowing for performing the sensory (visual) stimulation. In contrast, the snail ganglia and rat cell cultures used in previous *in vitro* ncMRI experiments (16–18) do not include the nervous system that perceives and processes physiological stimulation. By applying sodium-nitrosocystein and electrical stimulation to generate epileptiform neuronal activity in the snail ganglia, Park et al. (16, 17) found a magnitude MRI signal decrease of 5.49% and 2.97% at 3T, respectively. In a later report (26), based on their theoretical analysis, the same authors concluded that these signal changes are unlikely to be caused by the magnetic fields produced by the neuronal activity. In the rat cell culture study (18), MRI phase signal decreases of 0.15 to 3° were observed at 7T by suppressing the spontaneous neuronal activity with tetrodotoxin. Little information was provided from the previous *in vitro* studies for determining the likelihood of detecting and estimating the size of the ncMRI signals changes in the present study. The amplitude of ncMRI signal changes is closely related to the structure of neural networks (28) and the type of neuronal activities (evoked, spontaneous and epileptic event) (29). Differences in neural networking and stimulation tasks will affect both the number of neurons fired synchronously and the intensity of neural currents. The estimation of any new ncMRI experiments based on any previous experiments will only be meaningful if exact information is provided regarding the morphology and biophysical property of neurons, the electrophysiological characteristics of pre-synaptic and post-synaptic activity induced by the stimulation, and the synaptic connections in the neural network.

During the experiment, the turtle brains were bathed in Ringer's solution, which is oxygenated with 95% oxygen gas (O₂) and oxygen is transported into the tissue to supply its energy metabolism. Due to the paramagnetic property of O₂, the variation of neuronal activity can change the oxygen consumption rate and oxygen concentration, resulting in MRI signal changes (30). It was observed that oxygen consumption rate can be increased as much as 30% in response to an event-related stimulation paradigm (31). Based on the 30% oxygen consumption rate change, the upper limit of oxygen-induced MRI signal changes was estimated to be 0.02%/0.04° in magnitude/phase (30). Therefore, the detection sensitivity of ncMRI signals will depend on the oxygen effects and the lower limit of its detectability will be 0.02%/0.04° in magnitude/phase.

We showed results when the visual stimulation was delivered simultaneously to both eyes of the turtles (n=8). Also, in three of the eight turtles, we applied the stimulation to just one eye. Again, no ncMRI magnitude and phase signal changes associated with the visual-evoked activity were found in these single eye stimulation experiments. In turtle brain, the left and right cerebral cortex receive excitatory input entirely from the contralateral eye, so the intensity of neuronal activity in the left and right visual cortex would not change when stimulating one eye as compared to the stimulation of two eyes. When applying the stimulation to both eyes, considering that the apical dendrites of pyramidal neurons are approximately perpendicular to the cortical surface, a part of neuronal currents in the left and right dorsomedial/medial cortical areas (Fig. 2C) would be orientated in opposite directions, and then result in the cancellation of neuronal magnetic fields in the vicinity of the middle line of the cortex. When stimulating a single eye, the visual evoked neuronal activity was present in only one side of cortex, so the neuronal magnetic fields in the dorsomedial/medial cortical cortex would not be canceled. Therefore, the ncMRI signals in the dorsomedial/medial cortical cortex would be larger for one-eye stimulation compared with two-eye stimulation. However, the two-eye stimulation would not reduce the ncMRI signals in the visual cortex, because the pyramidal neurons in the left and right visual cortex

are approximately parallel. The results of optical imaging (voltage-sensitive dye) experiments (32) in turtles have shown that the most intense visual-evoked neuronal activity appears in the medial visual cortex, so the maximum ncMRI signals in the turtle brain should be located in the visual cortex. Thus, the possibility for detecting the maximum ncMRI signal changes in the turtle brain would be same for one-eye stimulation and two-eye stimulation.

A relative long and fixed inter-stimulus interval (ISI=16s) was used in the visual stimulation paradigm to ensure the consistent responses to all the visual stimuli. The visual-evoked neuronal response returned to the baseline within 1.6s after the stimulus onset. The ISI is much longer than the duration of the response. If we shortened the ISI, the duty cycle of the stimulation paradigm would be increased and the detection power would be improved. Unfortunately, short ISIs can not be implemented, because they induce considerable neuronal adaptation, which reduces the intensity of neuronal response significantly and even leads to the absence of visual evoked neuronal activity in visual cortex. We tested the ISI=5s and 10s, and found that the peak value of cortical LFP signals (averaged over 20 trials) decreased by approximately 62% and 28% compared to the LFP signals for ISI=16s, respectively. Furthermore, the intensity of neuronal responses varied significantly in different trials, and even no response was produced in some trials at the short ISIs. This would decrease the sensitivity and reliability for measuring the ncMRI signals. Thus, an ISI of 16s was chosen to ensure that the turtle brain produced strong and consistent neuronal responses to all the visual stimuli.

Full field flash has been the most used visual task in the study of turtle visual system over the past xx years. Using the full field flash in the present ncMRI experiments has scientific benefits in best utilizing the knowledge on the turtle visual neuronal activity gained by previous studies. In addition to the full field flash study, we also have measured the LFP signal on turtle brain in response to the checkerboard visual task (widely used in human studies), to determine whether or not it is able to produce less neuronal adaptation and stronger neuronal activity in turtle visual cortex than the full field flash does. The results from our comparison study show that the behavior of the neuronal adaptation for various ISIs in the turtle visual cortex is similar between checkerboard and full field flash stimulations (supporting information (SI) Fig. S1). In addition, there is no statistical difference in the peak amplitude of the LFP signal in turtle visual cortex between these two stimuli (Fig. S2). The continuous search of other visual tasks that may produce less neuronal adaptation and stronger neuronal responses is underway in our laboratory.

Although turtle and mammal brains share many characteristics, further investigation is needed to extend the conclusions of the present study to *in vivo* human ncMRI studies. The ncMRI signal changes depend on the neuronal currents in individual neurons and the degree of synchrony of their firing, which are related to morphology and biophysical properties of neurons and neural networking. It has been known that the morphology and electrophysiological properties of pyramidal neurons in turtles are similar to those in mammals (33, 34). Like mammals, turtles also have a layered cerebral cortex with a primary visual area (V1). Lateral geniculate neurons in the thalamus that receive direct excitatory input from retinal ganglion cells relay this visual information to both pyramidal cells and local inhibitory interneurons within V1 (35). However, although there is similarity in the visual information processing between turtles and mammals, the density of firing neurons induced by visual stimulation in turtles has not been measured through experiments. Further experiments and theoretical modeling need to be performed to quantitatively compare the ncMRI signals in turtle brains with that of human brains.

The results in this study indicate that the ncMRI signal induced by visual-evoked neuronal activity is beyond the detection capability (magnitude/phase=0.11%/0.09°) of our experimental design. To further improve the detection power of the ncMRI technology, one straightforward method is to increase the number of image averages. The prepared turtle brain can show stable neuronal response to visual stimulation for up to 72 hours, so more MRI images in turtles can be acquired. The detection power will be augmented through more averages (square root of N). Several imaging pulse sequences have been proposed for more effective measuring ncMRI signal, such as alternating balanced steady-state free precession (36) and stimulus-induced rotary saturation (37). An alternative proposal to detect the ncMRI is to use an extremely low magnet (10^{-6} T) so that the BOLD effects are negligible (38–40). By applying these new ideas and novel technology, more information regarding the order of ncMRI signals will be able to be determined experimentally.

Methods and Materials

Animal preparation

The experiments were performed on eight wild-caught adult pond turtles (*Pseudemys scripta*, Niles Biological, Sacramento, CA) with carapace lengths between 10 and 15cm. Use of the animals was approved by our institutional animal care and use committee. The surgery for isolating the complete brain from the turtle cranium with the eye attached has been detailed elsewhere (19, 32, 41). Briefly, a rectangular segment (approximately $4\times 3\text{cm}^2$) of plastron over the heart was removed from the anesthetized turtle with an electric hand drill, and then the pericardium was opened and the right atrium was incised. To remove the blood from the turtle brain's vasculature, the turtle was transcardially perfused through the ventricle with about 300ml of Ringer's solution. The Ringer's solution is an aCSF with the following composition (in mM): 96.5 NaCl, 2.6 KCl, 4 CaCl₂, 2 MgCl₂, 31.5 NaHCO₃ and 10 D-glucose, gassed to pH 7.6 with 95% O₂ and 5% CO₂. When the blood had been cleared from the body, the animal was rapidly decapitated. The brain with eyes attached was dissected from the cranium and placed in the recording chamber filled with Ringer's solution. It took approximately 3–4 hours in total to finish all the procedures of animal preparation. The dissection of turtle eye-brain was performed in Ringer's solution, which maintained the normal energy metabolism in the eye-brain.

Experimental setup

The experimental setup is shown in Fig. 3. During the LFP recording and ncMRI data acquisition, the turtle eye-brain preparation was placed in the recording chamber. The recording chamber was an open top box made of opaque plastic. The top of the chamber was closed by a lid with screws when the MRI image acquisition and LFP recording were performed. The recording chamber was secured in a customized animal holder, and the turtle brain and eyes were stabilized in the chamber with the plastic block and eye holder to minimize/eliminate any potential motion-related artifacts.

There were two tubings on the bottom of the chamber. Through one of the tubings, fresh Ringer's solution was perfused into the chamber continuously by a peristaltic pump (Mini Star, World Precision Instruments, Sarasota, FL). The excess solution flowed out of the chamber through the other tubing. A low perfusion speed ($\sim 1\text{mL}/\text{min}$) was used to ensure that the flow would not cause movement of the turtle brain. No artifacts induced by the perfusion process were observed in the MRI images acquired in this study. Also, the signal to noise ratio and temporal stability in the MRI images acquired with perfusion were comparable to that in the MRI images collected without perfusion.

A white LED source was used for visual stimulation. The onset and duration of white light flashes were controlled by the TTL pulses generated by E-Prime (Psychology Software Tools, Pittsburgh, PA). The visual stimuli were simultaneously delivered to both eyes of the turtle through two separate optical fiber bundles. The plastic tips of optical fiber bundles were inserted into the recording chamber and fixed with plastic screws (Fig. 3). The optical fiber tips were about 1 cm away from the eyes.

The LFP signals in the turtle brain were collected by placing the tips of two Teflon-coated silver wires on the brain and in the solution. The other tips of the silver wires were fixed on the chamber's wall and connected to a differential AC amplifier (A-M 1700, A-M Systems, Carlsborg, WA) located outside the 5-Gauss line and about 3 m from the scanner center. The LFP signals from amplifier were digitized and recorded.

Visual stimulation paradigm

An event-related visual stimulation paradigm was used in the LFP and ncMRI experiments. The duration of each stimulus (white light flash) was 50ms, and ISI=16s. The paradigm consisted of 20 and 141 trials for the LFP recording and ncMRI experiment, respectively (see Figs. 1A and 2B).

LFP data acquisition and processing

The LFP signals were recorded in the visual cortex and optic tectum of the turtle eye-brain preparations. The timing diagram of the LFP recordings is shown in Fig. 1A. The LFP recordings were performed at four points in the turtle brain (centers of left cortex, right cortex, left tectum, and right tectum) immediately before and after the MRI session. To further ensure that the visual stimulation induced neuronal electrical activity in the turtle brain during each MRI scan, the LFP signals at the center of either the left or right tectum were recorded interleaved with the MRI scans. The filter setting for the LFP amplifier was 1Hz low-cut and 1KHz high-cut. The LFP signal was averaged over the 20 trials to obtain the mean LFP time course of the visual stimulus-locked evoked neuronal activity. The neuronal response peak latency (time delay between the maximum response peak and the stimulus onset) and peak duration (full width at half maximum of the peak) were obtained from the mean LFP time courses.

ncMRI data acquisition

The ncMRI data were acquired on a Bruker 9.4T MRI scanner (Bruker, Karlsruhe, Germany) with a circular surface RF coil of 2.5cm diameter, using a single shot gradient echo EPI sequence with the following parameters: FOV=3×3cm², matrix size=64×64 (resolution≈0.47×0.47mm²), TR=2s, and rf pulse flip angle=65° (Ernst angle). Since the ncMRI signal change depends upon TE, six different TE values (=15 to 40ms with 5ms interval) were used to explore the possibility for detecting the ncMRI signal. It should be noted that the MRI data for different TEs were acquired from separate scans, and a fixed TE was used in an individual MRI scan. As Fig. 2A shows that the rostral-caudal (head-tail) direction of the turtle brain was positioned to be parallel to B₀, and therefore the surface of visual cortex was perpendicular to B₀. Since the dendrites of pyramidal neurons are approximately perpendicular to the cortical surface, the neuronal currents in the visual cortex are nearly perpendicular to B₀. This position would maximize the components of the magnetic fields generated by the neuronal currents on the direction of B₀, and result in the strongest ncMRI signals. Five 2mm thick axial image slices were selected to cover the whole cortex and tectum of turtle (Fig. 2A). Slices 4 and 2 were located at the central cortex and tectum, respectively. To allow the mapping of ncMRI data on an anatomical reference, the corresponding high-resolution T₂-weighted anatomical images were acquired using a

rapid acquisition with relaxation enhancement (RARE) sequence with TR=2s, TE=80ms, RARE factor=8, and matrix size=192×192.

The ncMRI acquisition strategy is shown in Fig. 2B. To capture the maximum ncMRI signal in the central visual cortex and optic tectum, a time delay (τ) was set between the start of visual stimulation and that of the MRI data acquisition. This ensured that the acquisition windows of slices 4 and 2 were located within the positive response peak of visual-evoked neuronal activity in the cortex and tectum, respectively. It should be noted that τ could vary in the experiments for different turtles, and was determined from LFP signals recorded (prior to MRI) in the individual turtle brains.

ncMRI data analysis

An ncMRI data set includes 141 trials and for each image slice there were 8 images in each trial. The first and the subsequent seven images in each trial were acquired during the visual-evoked neuronal activity (active state) and the baseline (resting state), respectively. Before analyzing the data sets, the images of the first trial (0–16s) were discarded to ensure that the MRI signal reached steady-state. To preserve the potential relative small activated foci (be well localized in the firing neurons) and nature of the ncMRI map, no spatial smoothing was applied to the MRI images (4). Both voxel-wise and ROI data analysis methods were used to detect the ncMRI signals in the MRI images as described below:

The voxel-wise analyses—Two strategies were adopted for the voxel-wise analysis: (1) Multiple comparison correction: For each slice and for each individual TE (15 to 40ms and 5ms interval), the magnitude/phase images were divided into two groups, which consisted of the images at active state (first image in each trial) and that at resting state (subsequent seven images in each trial), respectively. A t-map was obtained by performing a student's group t-test on the two groups of images. The activated voxels for both negative and positive signal changes were identified by thresholding the ncMRI t-maps with $p < 0.05$, Bonferroni corrected for multiple comparisons (42). Bonferroni correction would be more appropriate than Gaussian field correction for the data analysis in this study, because it is less severe when no spatial smoothing is applied to the MRI data (43). The voxels outside the brain region were removed and not considered in the further analysis. The number of voxels inside the brain region for each slice and for each turtle was varied, and it was in the range of 102–397. Thus, the threshold t-value corresponding to $p = 0.05$ corrected was in the range of 3.5–3.8. (2) Fast effect (FE) vs. control: For each slice and each individual TE, a FE t-map was obtained by applying a group t-test between the image group at active state and the one at resting state, which included the first image and the last six images in each trial, respectively. The corresponding control t-map was obtained by carrying out a group t-test on the two image groups both at resting state. These two groups were composed of the second image and subsequent six images in each trial, respectively. The FE and control t-maps were thresholded at $p < 0.05$ uncorrected. For each individual TE, the FE and control t-maps of the eight turtles were statistically compared in the number of voxels above the statistical threshold in the brain (5 slices) and the signal changes averaged over these voxels. Since all the “activated” voxels (voxels at $p < 0.05$ uncorrected) in the control t-maps should be attributed to random noise, if there was no statistically significant difference between the FE and control t-maps, the “activated” voxels in the FE t-maps would be considered to be induced by random noise just as the control t-maps does.

ROI analysis—In the magnitude/phase images of each individual TE, four ROIs in the cortex (slice 4) and one ROI in the tectum (slice 2) were selected to cover the brain areas (color regions in the schematic drawing in Figure 2C) involved in the visual-evoked neuronal activity. Each ROI in the cortex was composed of two sub-regions that cover the

two parts of a cortical area in the left and right brain. The ROI-averaged signals for each brain area and for the entire cortex were obtained by averaging the MRI signals inside each ROI and all the ROIs of cortex together. In addition, since the strongest visual-evoked neuronal activity should be present in the visual cortex, the ROI-averaged signals for the visual cortex were also obtained by averaging the MRI signals inside the ROIs of medial and lateral visual cortex together. Each ROI-averaged signal included 140 trials and 8 data points in each trial. To examine if there were significant ncMRI signal changes during the visual-evoked activity relative to the baseline, the MRI signals of the data points at active state (including the first data point in each trial) were compared with the ones at resting state (including data points 2–8 in each trial) using a group t-test ($p < 0.05$ uncorrected).

Supplementary Material

Refer to Web version on PubMed Central for supplementary material.

Acknowledgments

This work was supported by a NIH grant (RO1 EB004753 to JHG) and the Intramural Research Program of the NIH/NIDA.

Abbreviations

MRI	magnetic resonance imaging
EEG	electroencephalography
MEG	magnetoencephalography
PET	positron emission tomography
EPI	echo planar imaging

References

1. Kamei H, Iramina K, Yoshikawa K, Ueno S. Neuronal Current Distribution Imaging Using MR. *IEEE Trans On Magnetics*. 1999; 35:4109–4111.
2. Xiong J, Fox PT, Gao JH. Direct mapping magnetic field effects of neuronal activity by magnetic resonance imaging. *Hum Brain Mapp*. 2003; 20:41–49. [PubMed: 12953305]
3. Konn D, Leach S, Gowland P, Bowtell R. Initial attempts at directly detecting alpha wave activity in the brain using MRI. *Magn Reson Imaging*. 2004; 22:1413–1427. [PubMed: 15707791]
4. Bianciardi M, Di Russo F, Aprile T, Maraviglia B, Hagberg GE. Combination of BOLD-fMRI and VEP recording for spin-echo MRI detection of primary magnetic effects caused by neuronal currents. *Magn Reson Imaging*. 2004; 22:1429–1440. [PubMed: 15707792]
5. Liston AD, Salek-Haddaki A, Kiebel SJ, Hamandi K, Turner R, Lemieux L. The MR detection of neuronal depolarization during 3-Hz spike-and-wave complexes in generalized epilepsy. *Magn Reson Imaging*. 2004; 22:1441–1444. [PubMed: 15707793]
6. Chow LS, Cook GG, Whitby E, Paley MNJ. Investigating direct detection of axon firing in the adult human optic nerve using MRI. *NeuroImage*. 2006; 30:835–846. [PubMed: 16376108]
7. Chow LS, Cook GG, Whitby E, Paley MNJ. Investigation of MR signal modulation due to magnetic fields from neuronal currents in the adult human optic nerve and visual cortex. *Magn Reson Imaging*. 2006; 24:681–691. [PubMed: 16824962]
8. Chow LS, Cook GG, Whitby E, Paley MNJ. Investigation of axonal magnetic fields in the human corpus callosum using visual stimulation based on MR signal modulation. *J Magn Reson Imaging*. 2007; 26:265–273. [PubMed: 17654726]

9. Chow LS, Dagens A, Fu Y, Cook GG, Paley MNJ. Comparison of BOLD and direct-MR neuronal detection (DND) in the human visual cortex at 3T. *Magn Reson Med*. 2008; 60:1147–1154. [PubMed: 18956466]
10. Singh M. Sensitivity of MR phase shift to detect evoked neuromagnetic fields inside the head. *IEEE Trans Nucl Sci*. 1994; 41:349–351.
11. Chu R, de Zwart JA, Gelderen PV, Fukunaga M, Kellman P, Holroyd T, Duyn JH. Hunting for neuronal currents: absence of rapid MRI signal changes during visual-evoked response. *NeuroImage*. 2004; 23:1059–1067. [PubMed: 15528106]
12. Parkes LM, de Lange FP, Fries P, Toni I, Norris DG. Inability to directly detect magnetic field changes associated with neuronal activity. *Magn Reson Med*. 2007; 57:411–416. [PubMed: 17260380]
13. Mandelkow H, Halder P, Brandeis D, Soellinger M, de Zanche N, Luechinger R, Boesiger P. Heart beats brain: The problem of detecting alpha waves by neuronal current imaging in joint EEG-MRI experiments. *NeuroImage*. 2007; 37:149–163. [PubMed: 17544703]
14. Tang L, Avison MJ, Gatenby JC, Gore JC. Failure to directly detect magnetic field dephasing corresponding to ERP generation. *Magn Reson Imaging*. 2008; 26:484–489. [PubMed: 18180125]
15. Bandettini PA, Petridou N, Bodurka J. Direct detection of neuronal activity with MRI: Fantasy, possibility, or reality? *Appl Magn Reson*. 2005; 29:65–88.
16. Park TS, Lee SY, Park JH, Lee SY. Effect of nerve cell currents on MRI images in snail ganglia. *NeuroReport*. 2004; 15:2783–2786. [PubMed: 15597054]
17. Park TS, Lee SY, Park JH, Cho MH, Lee SY. Observation of the fast response of a magnetic resonance signal to neuronal activity: a snail ganglia study. *Physiol Meas*. 2006; 27:181–190. [PubMed: 16400204]
18. Petridou N, Plenz D, Silva AC, Loew M, Bodurka J, Bandettini PA. Direct magnetic resonance detection of neuronal electrical activity. *Proc Natl Acad Sci USA*. 2006; 103:16015–16020. [PubMed: 17038505]
19. Kriegstein AR. Synaptic responses of cortical pyramidal neurons to light stimulation in the isolated turtle visual system. *J Neurosci*. 1987; 7:2488–2492. [PubMed: 3612249]
20. Fan TX, Rosenberg AF, Ariel M. Visual-response properties of units in the turtle cerebellar granular layer in vitro. *J Neurophysiol*. 1993; 4:1314–1322. [PubMed: 8492165]
21. Murphy K, Bodurka J, Bandettini PA. How long to scan? The relationship between fMRI temporal signal to noise ratio and necessary scan duration. *Neuroimage*. 2007; 34:565–574. [PubMed: 17126038]
22. Bodurka J, Jesmanowicz A, Hyde JS, Xu H, Estkowski L, Li SJ. Current-induced magnetic resonance phase imaging. *J Magn Reson*. 1999; 137:265–271. [PubMed: 10053158]
23. Bodurka J, Bandettini PA. Toward direct mapping of neuronal activity: MRI detection of ultraweak, transient magnetic field changes. *Magn Reson Med*. 2002; 47:1052–1058. [PubMed: 12111950]
24. Konn D, Gowland P, Bowtell R. MRI detection of weak magnetic fields due to an extended current dipole in a conducting sphere: a model for direct detection of neuronal currents in the brain. *Magn Reson Med*. 2003; 50:40–49. [PubMed: 12815677]
25. Xue Y, Gao JH, Xiong J. Direct MRI detection of neuronal magnetic fields in the brain: theoretical modeling. *Neuroimage*. 2006; 31:550–559. [PubMed: 16504542]
26. Park TS, Lee SY. Effects of neuronal magnetic fields on MRI: numerical analysis with axon and dendrite models. *Neuroimage*. 2007; 35:531–538. [PubMed: 17291782]
27. Blagoev KB, Mihaila B, Travis BJ, Alexandrov LB, Bishop AR, Ranken D, Posse S, Gasparovic C, Mayer A, Aine CJ, Ulbert I, Morita M, Muller W, Connor J, Halgren E. Modeling the magnetic signature of neuronal tissue. *Neuroimage*. 2007; 37:137–148. [PubMed: 17544300]
28. Cassara AM, Hagberg GE, Bianciardi M, Migliore M, Maraviglia B. Realistic simulations of neuronal activity: a contribution to the debate on direct detection of neuronal currents by MRI. *Neuroimage*. 2008; 39:87–106. [PubMed: 17936018]
29. Hagberg GE, Bianciardi M, Maraviglia B. Challenges for detection of neuronal currents by MRI. *Magn Reson Imaging*. 2006; 24:483–493. [PubMed: 16677955]

30. Luo Q, Liu HL, Parris B, Lu H, Senseman DM, Gao JH. Modeling oxygen effects in tissue preparation neuronal current MRI. *Magn Reson Med*. 2007; 58:407–412. [PubMed: 17654581]
31. Kennedy RT, Jones SR, Wightman RM. Simultaneous measurement of oxygen and dopamine: coupling of oxygen consumption and neurotransmission. *Neuroscience*. 1992; 47:603–612. [PubMed: 1316568]
32. Senseman DM. Spatiotemporal structure of depolarization spread in cortical pyramidal cell populations evoked by diffuse retinal light flashes. *Vis Neurosci*. 1999; 16:65–79. [PubMed: 10022479]
33. Connors BW, Kriegstein AR. Cellular physiology of the turtle visual cortex: distinctive properties of pyramidal and stellate neurons. *J Neurosci*. 1986; 6:164–177. [PubMed: 3944618]
34. Larkum, Watanabe S, Lasser-Ross N, Rhodes P, Ross WN. Dendritic properties of turtle pyramidal neurons. *J Neurophysiol*. 2008; 99:683–694. [PubMed: 18045998]
35. Ulinski, PS. Cerebral Cortex. Jones, EG.; Peters, A., editors. Plenum; New York: 1990. p. 307-324.
36. Buracas GT, Liu TT, Buxton RB, Frank LR, Wong EC. Imaging periodic currents using alternating balanced steady-state free precession. *Magn Reson Med*. 2008; 59:140–148. [PubMed: 18050317]
37. Witzel T, Lin FH, Rosen BR, Wald LL. Stimulus-induced Rotary Saturation (SIRS): a potential method for the detection of neuronal currents with MRI. *Neuroimage*. 2008; 42:1357–1365. [PubMed: 18684643]
38. Volegov P, Matlachov AN, Espy MA, George JS, Kraus RH. Simultaneous magnetoencephalography and SQUID detected nuclear MR in microtesla magnetic fields. *Magn Reson Med*. 2004; 52:467–470. [PubMed: 15334563]
39. Espy MA, Matlachov AN, Volegov PL, Mosher JC, Kraus RH. SQUID-Based Simultaneous Detection of NMR and Biomagnetic Signals at Ultra-Low Magnetic Fields. *IEEE Trans Appl Supercond*. 2005; 15:635–639.
40. Zotev VS, Matlashov AN, Volegov PL, Savukov IM, Espy MA, Mosher JC, Gomez JJ, Kraus RH. Microtesla MRI of the human brain combined with MEG. *J Magn Reson*. 2008; 194:115–120. [PubMed: 18619876]
41. Senseman DM. Correspondence between visually evoked voltage-sensitive dye signals and synaptic activity recorded in cortical pyramidal cells with intracellular microelectrodes. *Vis Neurosci*. 1996; 13:963–977. [PubMed: 8903037]
42. Brett, M.; Penny, WD.; Kiebel, SJ. Human Brain Function. Frackowiak, RS.; Friston, KJ.; Frith, CD.; Dolan, R.; Price, CJ.; Zeki, S.; Ashburner, J.; Penny, WD., editors. Academic Press; New York: 2003. p. 867-879.
43. Worsley KJ, Friston KJ. Analysis of fMRI time-series revisited—again. *Neuroimage*. 1995; 2:173–181. [PubMed: 9343600]

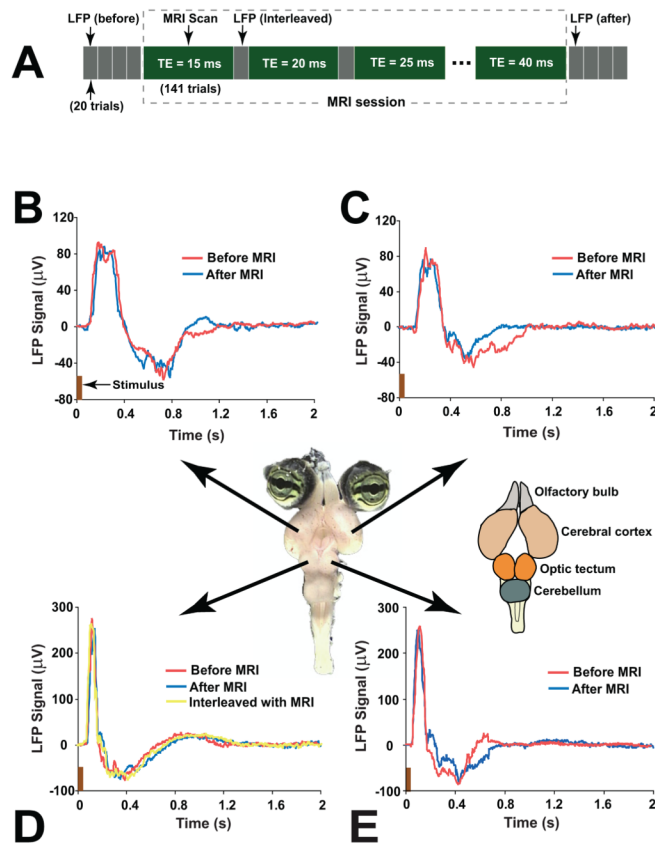


Figure 1.

(A) The timing diagram of LFP recording and MRI data acquisition. Before and after the MRI session, four LFP recordings (20 trials for each recording) were performed at the center part of left, right cortex and tectum, respectively. During the MRI session, an interleaved LFP/MRI acquisition was performed. An MRI session was composed of six MRI scans (141 trials per scan), and each MRI scan used a different and fixed TE (TE=15–40ms with interval of 5ms). The single channel LFP signal in either the left or right central tectum was collected between any two adjacent MRI scans. (B–E): Visual-evoked LFP signals measured immediately before and after the MRI scan in the left (B) and right (C) visual cortex, and left (D) and right (E) optic tectum of the turtle brain. A LFP trace recorded interleaved with the MRI scans is shown in (D). The picture in the middle shows an isolated turtle eye-brain, and the major parts (olfactory bulb, cerebral cortex, optic tectum, and cerebellum) of turtle brain are indicated in the schematic drawing on the right of the picture.

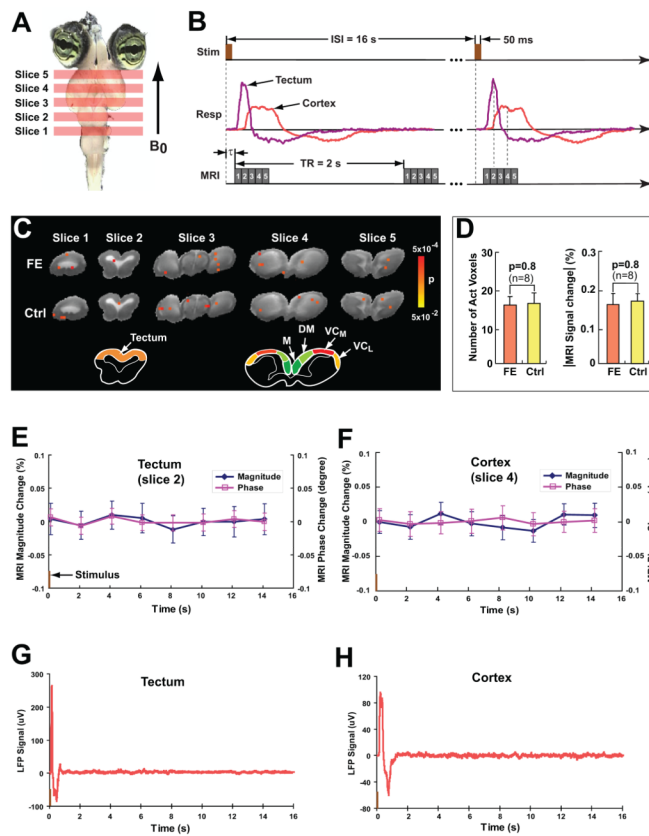


Figure 2.

(A) The slice location in the MRI data acquisition. (B) The time diagram of ncMRI data acquisition. (C) The fast effect (FE) and control (Ctrl) t-maps ($p < 0.05$ uncorrected) of negative signal changes overlaid on the T_2 -weighted anatomical images. The t-maps were obtained from the magnitude images of $TE = 20$ ms in a single turtle. The schematic drawing below the maps shows the major brain areas of cortex and tectum in slices 4 and 2, respectively. The cortical areas include medial cortex (M), dorsomedial cortex (DM), medial visual cortex (VC_M), and lateral visual cortex (VC_L). (D) The statistical comparison between the FE and control t-maps of negative magnitude signal changes in terms of the total number of “activated” voxels (voxels at $p < 0.05$) and the MRI percent signal change (absolute value) averaged over the “activated” voxels. (E) and (F) show the ROI-averaged signals (averaged over 140 trials) in the optic tectum and visual cortex ($VC_M + VC_L$) in a single turtle, respectively. The corresponding LFP traces (averaged over 20 trials) are shown in (G) and (H), respectively. In (E)–(H), the visual stimulus onsets at 0s and the stimulus duration is 50ms.

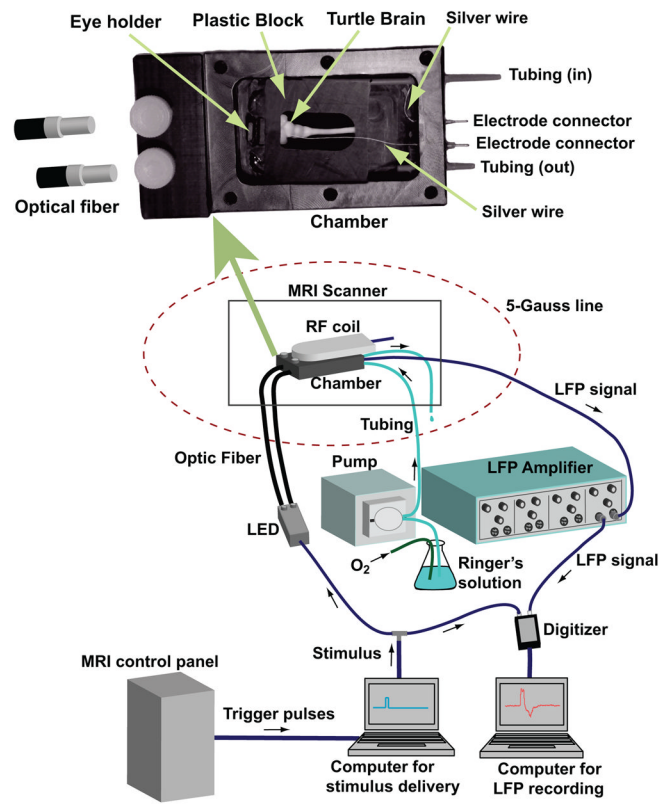


Figure 3.
The diagram of experimental setup and the design of recording chamber.